Published in partnership with King Fahd University of Petroleum & Minerals



https://doi.org/10.1038/s41545-025-00477-z

Novel ferromagnetic CuFe₂O₄/Cu as a highly active catalyst for microwave-Fenton-like reaction

Check for updates

Yejin Nam¹, Deukhyeon Nam²³, Yoon Myung², Jong Hoon Joo¹ & Changwoo Kim¹⊠

To overcome the short retention time in small-scale wastewater treatment plants, it is necessary to develop processes with fast reaction rates. The microwave-Fenton-like reaction (MW-Fenton-like reaction), which combines external energy and catalysts, provides a solution with rapid reaction rate and high degradation efficiency. In this reaction, catalysts significantly influence decomposition efficiency. Developing magnetic catalysts can simplify the separation process. In this study, the superiority of copper-based metal oxides for the MW-Fenton-like reaction was confirmed through comparative experiments of various metal oxides. Based on these findings, highly active $CuFe_2O_4/Cu$ particles were developed. The synthesized particles, with rough-surfaced solid-sphere morphology, exhibited ferromagnetic properties and were completely separated using a laboratory-scale magnet. $CuFe_2O_4/Cu$ also showed high degradation over a wide pH range and achieved the highest degradation rate at pH 7. Furthermore, comparison of 4-nitrophenol (4-NP) degradation using MW and conventional heating demonstrated MW was superior in reaction rate, efficiency, and reusability.

According to the effluent discharge regulations enforced globally, it is essential for wastewater generated by various industries such as pharmaceuticals, cosmetics, and textiles to be treated at wastewater treatment facilities, which are predominantly small in scale^{1–5}. However, these small-scale facilities often face issues with treatment efficiency due to short hydraulic retention times⁶. To meet the increasingly strict effluent standards, there is a direct need to address the constraints of limited hydraulic retention time and improve treatment efficiency.

In industrial wastewater treatment, one of the most widely used reactions is the Fenton reaction, which is particularly effective in degradation of refractory organic pollutants⁷. This reaction is classified as an advanced oxidation process (AOP), a group of chemical treatment methods that generate highly reactive radicals—such as hydroxyl (·OH) or sulfate (·SO₄') radicals—to non-selectively oxidize and mineralize a broad range of organic contaminants⁸. In the Fenton reaction, contaminants are degraded by radicals generated by the reaction between Fe²⁺/Fe³⁺ and H_2O_2 . However, since a strongly acidic environment (pH<3) is needed for the efficient degradation of pollutants, pH adjustment processes and a large quantity of chemicals are required to match both the optimal process pH and the effluent discharge regulations pH^{10,11}. Moreover, the Fenton reaction produces iron sludge, necessitating additional processes and treatment costs for removal¹². To address the issues of pH dependence and sludge generation in

the Fenton reaction, the Fenton-like reaction has been studied by replacing Fe²⁺/Fe³⁺ with an insoluble solid catalyst¹³. Furthermore, recent research has been conducted on the introducing external energy sources into the Fentonlike reaction, not only to overcome the limitations of the Fenton reaction but also to enhance the reaction kinetics^{14,15}. External energies, such as microwaves (MW), light, and vibrations, play a role in increasing the number of reactant particles able to overcome the activation energy barrier^{16,17}. MW, which refers to electromagnetic fields with frequencies ranging from 300 MHz to 300 GHz, is gaining attention for its rapid heating, non-contact heating, and the formation of hotspots with temperatures higher than their surroundings^{18,19}. Moreover, MW reduces the amount of energy required per unit mass (W/g) for processing as the total mass being treated increases, regardless of the process type, equipment used, or operating conditions²⁰. This indicates that the efficiency of MW increases with scale, highlighting its practical feasibility for large-scale processing operations. The combination of MW with an appropriate catalyst enables rapid heating rates and lowers the activation energy, leading to accelerated treatment speeds and high degradation efficiency^{21,22}.

To achieve high activity in MW-Fenton-like reactions, the catalyst must have a high MW absorption capacity and strong intrinsic reactivity of Fenton-like reaction. Various studies over the past decade have confirmed the high reactivity of Cu-based catalysts in MW-Fenton-like reactions^{23–54}.

A table summarizing these studies is attached in Supplementary information (Supplementary Table 1). Wang et al. and Iboukhoulef et al. used Cu^{2+} ions as catalysts for the MW-Fenton-like reaction^{23,24}. Additionally, solid-phase Cu-based oxides such as CuO, Cu₂O, CuFeO₂, CuCo₂O₄, and Cu-Ni bimetallic oxide have also been studied as catalysts for the MW-Fenton-like reactions^{25–32,34,36}. Cu-based catalysts integrated with carbon-based materials like graphene oxide, activated carbon, and biochar to enhance MW absorption capacity have also gained attention for MW-assisted processes^{41–43,45–55}. While these Cu-based catalysts exhibit excellent degradation efficiency and fast reaction rates, they present challenges in separating the catalysts after the degradation process⁵⁶. Developing magnetic particles such as MFe₂O₄ (where M = Fe, Cu, or Co) addresses these challenges by allowing for easy separation under a magnetic field^{27,33,37,40,45,52}. Magnetic separation can simplify the process, reduce separation time, and promote the reuse of catalysts^{57,58}.

 $CuFe_2O_4$ is gaining attention as a catalyst for MW-Fenton-like reactions due to its intrinsic magnetic properties and the presence of catalytically active copper species. $CuFe_2O_4$, a spinel ferrite nanoparticle (SFNP) with the general formula AB_2O_4 , exhibits excellent magnetic and structural stability, and its properties can be tailored by adjusting synthesis and calcination conditions 59,60 . Bose et al. synthesized a nanoflower-shaped catalyst by loading $CuFe_2O_4$ onto MoS_2 to enhance MW absorption capacity 33 . Xiao et al. loaded $CuFe_2O_4$ onto powdered activated carbon (PAC) to improve the catalyst's stability 40 . Yao et al. developed $CuFe_2O_4$ /reduced graphene oxide ($CuFe_2O_4$ /rGO), taking advantage of the high electronic conductivity of rGO to enhance the redox cycle in MW-Fenton-like reactions 44 . These $CuFe_2O_4$ -based catalysts can be used under various pH conditions, but they exhibit optimal efficiency in strongly acidic environments and tend to show decreased efficiency after several repeated reactions.

In this study, to enhance the efficiency of $CuFe_2O_4$, a spherical $CuFe_2O_4/Cu$ composite incorporating a zero-valent copper (Cu^0) phase, recognized for its strong reactivity toward organic pollutant removal, was synthesized for its strong reactivity toward organic pollutant removal, was synthesized for its strong reactivity toward organic pollutant removal, was synthesized for a pharmaceuticals, was used as a model pollutant to assess the degradation performance of the synthesized catalyst for conducted to evaluate the degradation performance under various experimental conditions and to determine the 4-NP degradation pathway. The synthesized $CuFe_2O_4/Cu$ showed optimal efficiency at neutral pH, eliminating the need for pH adjustment. Additionally, when comparing the activation of the catalyst using MW and conventional heating, only the MW-activated catalyst demonstrated complete reusability.

Results

Reactivity of metal oxides as catalysts for MW-Fenton-like reaction

MW energy absorbed by the catalyst can be converted into other forms of energy and used in the Fenton-like reaction. Therefore, MW absorption capacity of the catalyst is a key factor in selecting an appropriate catalyst for the MW-Fenton-like reaction. MW absorption is achieved through mechanisms such as magnetic loss and dielectric loss, among others⁶³. Metal oxides, which primarily rely on magnetic loss, are notable materials for MW absorption⁶⁴. Previous research has shown that MW absorption capacity improves as the number of metal components and the structural complexity of metal oxides⁶⁵. While many studies has focused on the influence of metal component number and morphology, more investigation is required to understand the impact of different metal types^{55,66}. To investigate the degradation rates based on metal types, an experiment was conducted using 21 different commercial metal oxides to degrade 4-NP (Fig. 1). A variety of metals were used, including an alkaline earth metal (Mg), transition metals (Ti, V, Cr, Mn, Fe, Co, Ni, Cu, Y, Zr, Nb, and Hf), lanthanides (La, Ce, and Gd), and post-transition metals (Al, Sn, and Bi). To account for surface area differences due to size, the hydrodynamic diameter was measured at pH 7 (Supplementary Fig. 1). The particle sizes ranged from 406 nm to 4.947 µm, contributing to variability in surface area among the samples. Among the 21 different metal oxides, copper oxide was the only material to exhibit

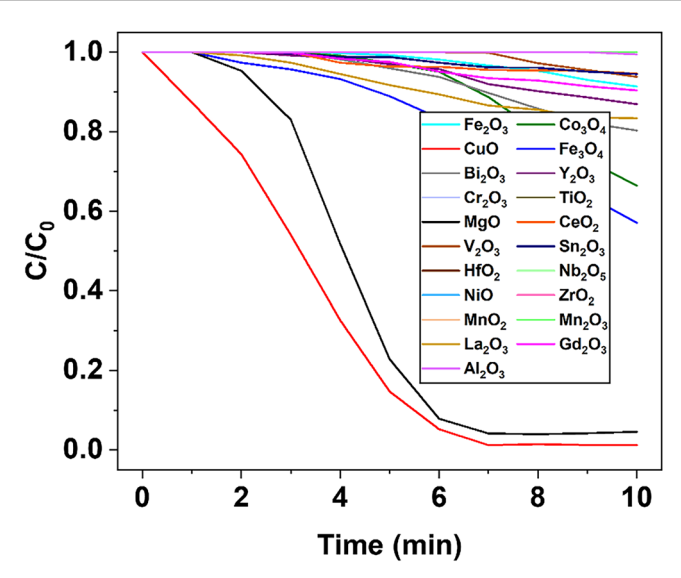


Fig. 1 | Degradation of 4-NP by MW-Fenton-like reaction with various monometallic oxide (Initial experimental condition: Cat. 200 ppm, H_2O_2 300 ppm, 4-NP 10 ppm, 20 °C, pH 7, and 200 W).

significant efficiency by degrading the majority of 4-NP within 10 min, despite variations in surface area. Despite not having the largest surface area or the highest MW absorption capacity, copper oxide exhibited high efficiency, likely due to its strong reactivity in the Fenton-like reaction is as equally important as MW absorption capability. While magnesium oxide demonstrated a relatively high degradation rate, it failed to achieve complete degradation of 4-NP. Additionally, a significant loss of catalyst was observed in the reactor following the reaction. This observation indicates that catalyst dissolution occurs during the reaction, confirming the extremely low stability and reusability of magnesium oxide. Considering the stability and degradation efficiency of the catalysts, copper oxide appears to be the most suitable choice for MW-Fenton-like reactions.

A dual-phase CuFe₂O₄ was synthesized by modifying the magnetic compound CuFe₂O₄. By adding CTAB and adjusting the heating temperature (300 °C or 350 °C) and gas conditions (Ar or O₂), CuFe₂O₄, CuFe₂O₄/Fe₂O₃, and CuFe₂O₄/Cu were synthesized. In contrast, CuFe₂O₄/CuO was synthesized under similar condition without using CTAB. All four synthesized CuFe₂O₄ samples exhibited a spherical shape. The surfactant CTAB acted as a template, resulting in CuFe₂O₄, CuFe₂O₄/Fe₂O₃, and CuFe₂O₄/Cu being approximately 40% smaller in size compared to CuFe₂O₄/CuO (Supplementary Fig. 2). XRD measurements revealed that all samples displayed peaks corresponding to CuFe₂O₄ (Fig. 2). In addition, CuFe₂O₄/Fe₂O₃, CuFe₂O₄/Cu, and CuFe₂O₄/CuO showed additional peaks corresponding to Fe₂O₃, Cu, and CuO, respectively. When O₂ or air was used as the synthesis atmosphere, additional metal oxide phases such as Fe₂O₃ or CuO were present. However, when Ar was used, only single-phase CuFe₂O₄ or additional metallic Cu phases were observed. This phenomenon is likely due to the lack of oxygen in the gas atmosphere.

Since catalysis occurs on the surface of the catalyst, the hydrodynamic diameter serves as a critical parameter influencing the accessible surface area. $CuFe_2O_4$, $CuFe_2O_4/Fe_2O_3$, and $CuFe_2O_4/CuO$ have comparable hydrodynamic diameters, while $CuFe_2O_4/Cu$ has a larger hydrodynamic diameter, leading to a relatively smaller surface area (Supplementary Fig. 3a). Despite the smaller surface area, $CuFe_2O_4/Cu$ exhibited a faster degradation rate of 4-NP compared to $CuFe_2O_4$, $CuFe_2O_4/Fe_2O_3$, and $CuFe_2O_4/CuO$ (Supplementary Fig. 3b). The elevated degradation rate of $CuFe_2O_4/Cu$ is attributed to efficient electron transfer driven by the presence of copper in multiple oxidation states. Based on these experimental results, subsequent experiments focused on $CuFe_2O_4/Cu$ as the primary catalyst. TEM images revealed that $CuFe_2O_4/Cu$ has a solid spherical

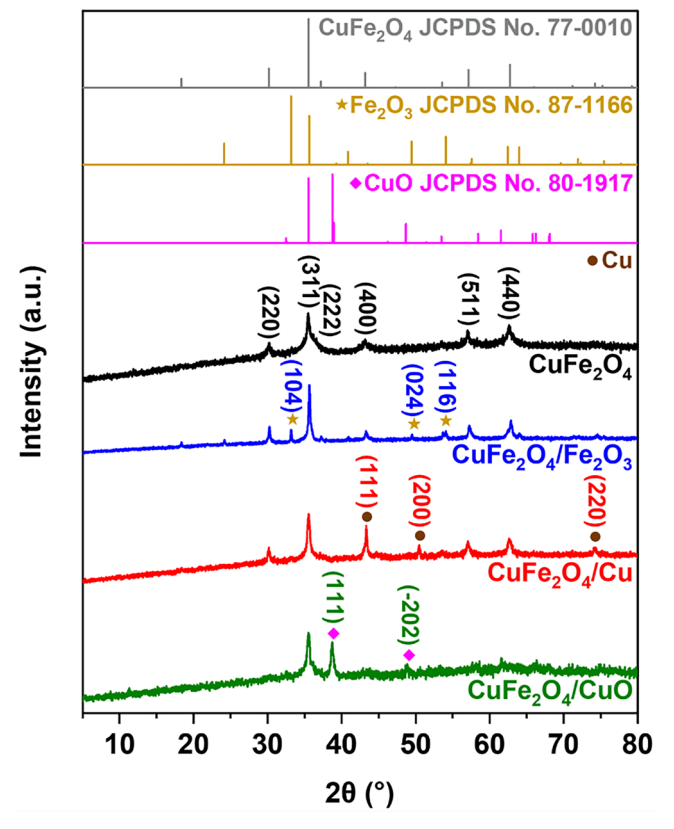


Fig. 2 | XRD of synthesized copper iron oxide: $CuFe_2O_4$, $CuFe_2O_4/Fe_2O_3$, $CuFe_2O_4/Cu$, and $CuFe_2O_4/CuO$. The peaks of Fe_2O_3 , Cu, and CuO were represented by yellow stars, brown circles, and pink diamond symbols, respectively.

structure with a rough surface (Fig. 3a, b). The rough surface could be one of the factors increasing the surface area, thus enhancing the reactivity with $H_2O_2^{68}$. The crystallinity of $CuFe_2O_4$ in $CuFe_2O_4/Cu$ was also confirmed by high-magnification TEM images showing a 0.252 nm interplanar spacing, corresponding to the (311) plane of $CuFe_2O_4$ (Fig. 3c). Additionally, the uniform distribution of all elements confirmed that the Cu peak observed in the XRD pattern did not originate from copper clusters (Fig. 3d–g).

An experiment was conducted to compare the efficiency of the synthesized CuFe₂O₄/Cu with commercial products (Fig. 4a). As commercial CuFe₂O₄/Cu was not available, an indirect comparison was conducted using commercial CuO, Fe₃O₄, and CuFe₂O₄. The commercial Fe₃O₄ showed a degradation rate of less than 50% even after 10 min of reaction, whereas the copper-containing commercial CuO and CuFe₂O₄ degraded most of the 4-NP. Additionally, the synthesized CuFe₂O₄/Cu demonstrated the highest efficiency, despite having a particle size more than four times greater than the commercial CuFe₂O₄. This suggests that the synthesized CuFe₂O₄/Cu exhibits high efficiency due to the synergistic effect between Cu⁰ and CuFe₂O₄, despite its simple structure and large size. Furthermore, the synthesized CuFe2O4/Cu based on magnetic CuFe2O4 was expected to possess magnetism, which was confirmed through experimentation (Fig. 4b). The magnetic property was easily observed by separating the catalyst in DI water using a magnet, and also confirmed by the SQUID measurement at 295 K. The saturation magnetization value of the synthesized particles was found to be 37.018 emu/g, and the irreversible narrow hysteresis loop indicated that the CuFe₂O₄/Cu is a soft magnetic material.

Effect of reaction factor on MW-Fenton-like reaction

The removal of 4-NP can occur through various pathways, including the self-decomposition of H_2O_2 , adsorption by $CuFe_2O_4/Cu$, and Fenton-like reaction. Experiments were performed to evaluate the impact of MW irradiation on 4-NP removal in each reaction pathway (Fig. 5). The self-

decomposition of H_2O_2 , adsorption by $CuFe_2O_4/Cu$, and the Fenton-like reaction achieved degradation rates of 0, 10, and 26%, respectively. While MW alone was unable to degrade the contaminant, its incorporation enhanced the degradation rates in all cases. In particular, the addition of MW to the Fenton-like reaction resulted in the greatest enhancement in both degradation efficiency and reaction rate. The majority of 4-NP was degraded within 5 min under MW irradiation. These results indicate that the majority of 4-NP degradation during the MW-Fenton-like reaction is driven by the Fenton-like reaction itself, rather than by the self-decomposition of H_2O_2 or adsorption by $CuFe_2O_4/Cu$.

The concentration of 4-NP, MW power, CuFe₂O₄/Cu concentration, H₂O₂ concentration, initial solution temperature, and pH are factors that influence the efficiency of the MW-Fenton-like reaction. To determine the optimal reaction conditions, experiments were conducted to assess the effects of these variables. The impact of pollutant concentration was investigated by measuring degradation rates across a range of 5-80 ppm (Fig. 6a). Complete degradation was observed within 5 min for 5 ppm and 10 ppm, while concentrations of 20 ppm or higher required 6 min. The degradation rate decreased as the pollutant concentration increased, likely because the amount of generated OH was limited. The amount of energy applied influences the number of reactant particles that can overcome the activation barrier, as shown in Fig. 6b. Degradation of 4-NP took 5, 3, 3, 2, and 2 min at 200, 400, 600, 800, and 1000 W, respectively. Although the reaction time decreased with increasing MW power, 200 W provided the best efficiency considering the total energy input required for complete degradation. The concentration of CuFe₂O₄/Cu affects the number of active sites available, so degradation performance was evaluated over the range of 20-400 ppm (Fig. 6c). To account for potential catalyst aggregation at high concentrations, hydrodynamic diameter measurements were also taken (Supplementary Fig. 4). The hydrodynamic diameter significantly increased from 20 ppm to 200 ppm and remained relatively constant above 200 ppm. The time required for 4-NP degradation at different catalyst concentrations was 9 min for 20 ppm and 40 ppm, 7 min for 100 ppm, and 5 min for 200 ppm and higher. The increase in reaction rate with catalyst concentration was likely due to the increase in active sites outweighing the decrease in surface area caused by aggregations.

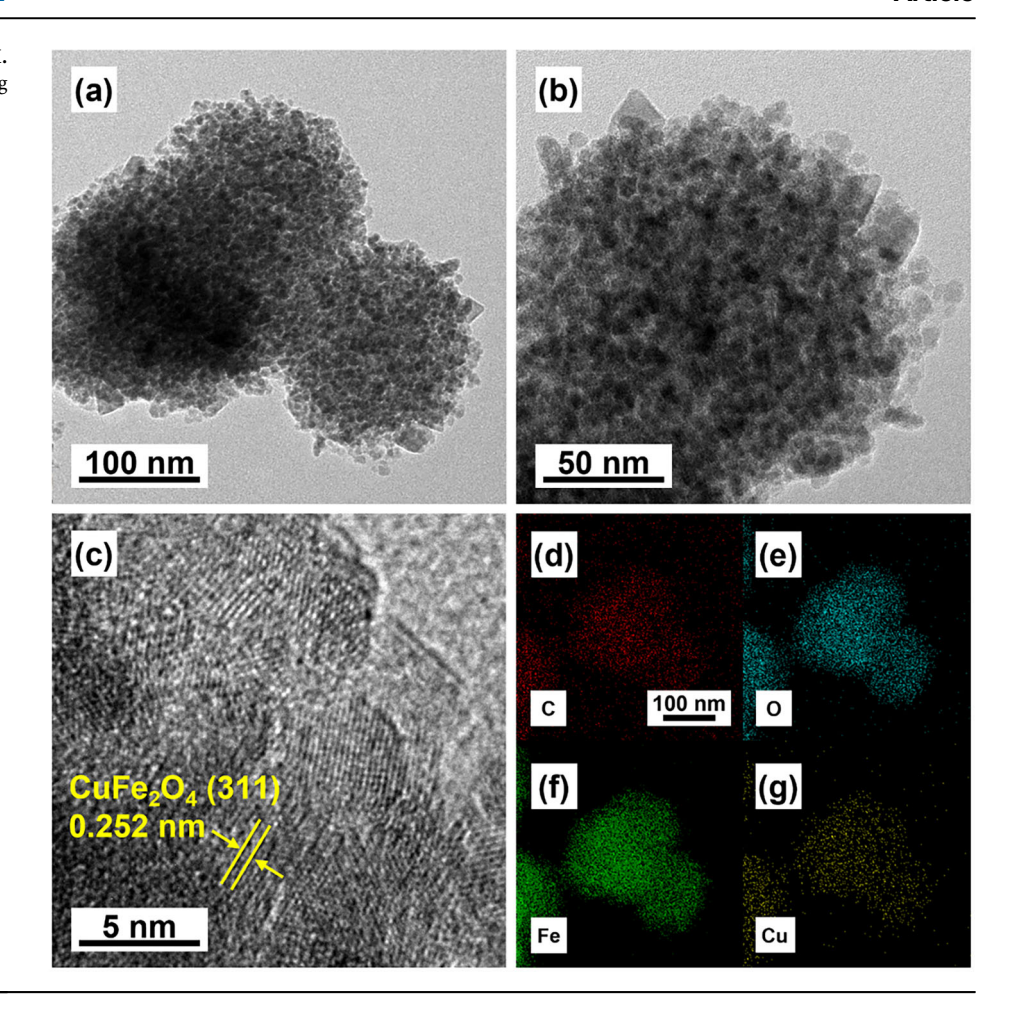
A controlled experiment was carried out to investigate the impact of H₂O₂ concentration on the decomposition rate (Fig. 6d). Before the main experiment, an experiment was conducted to account for the impact of H₂O₂ self-decomposition, as shown in Supplementary Fig. 5. The highest degradation rate due to self-decomposition was observed at 100 ppm, reaching 47%, indicating that H₂O₂ alone cannot completely degrade 4-NP. However, the combination of CuFe₂O₄/Cu with H₂O₂ resulted in substantial degradation. The reaction rate increased when the H₂O₂ concentration was raised from 100 ppm to 200 ppm. However, concentrations of 300 ppm or higher resulted in longer degradation times and a slight decrease in 4-NP removal efficiency. The decreased degradation rate, despite higher H₂O₂ concentrations, is likely due to the occurrence of side reactions where H₂O₂ acts as a scavenger of ·OH (Eqs. 1 and 2)⁶⁹. These side reactions not only consume two ·OH per H₂O₂ molecule but also reduce the amount of H2O2 available for generating ·OH, effectively consuming four ·OH per side reaction.

$$H_2O_2 + \cdot OH \rightarrow \cdot HO_2 + H_2O$$
 (1)

$$\cdot OH + \cdot HO_2 \rightarrow H_2O + O_2 \tag{2}$$

As the MW-Fenton-like reaction proceeds, the heating effect causes the solution temperature to reach the boiling point of water (100 °C) (Supplementary Fig. 6). Since the solution temperature can affect the degradation rate by modifying the activation energy, experiments were carried out to examine its influence. It was impossible to maintain a constant temperature throughout the reaction time due to the structure of the batch experimental system. Therefore, experiments were conducted by varying the initial solution temperature from 20 °C to 100 °C (Fig. 6e). The increase in the

Fig. 3 | Characterization of CuFe₂O₄/Cu by TEM. a-c TEM images of CuFe₂O₄/Cu and EDS mapping images of d C, e O, f Fe, and g Cu in CuFe₂O₄/Cu. EDS mapping images share the same scale bar.



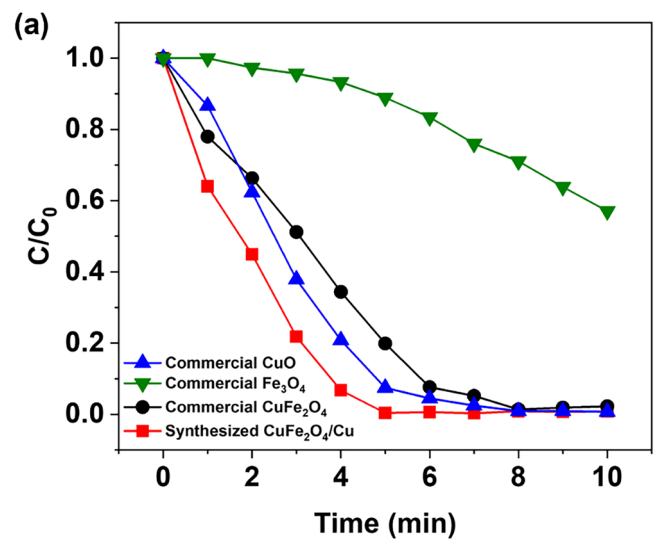
initial solution temperature from 20 °C to 100 °C resulted in a reduction in activation energy, thereby enhanced the degradation rate of 4-NP. Furthermore, kinetic analysis based on the initial solution temperatures revealed that the reaction follows pseudo first-order kinetics, and the rate constant increases with rising initial solution temperature (Supplementary Table 2). To isolate the effect of increased temperature and examine the impact of MW-specific characteristics, such as hotspot generation, 4-NP degradation experiments were conducted using conventional heating (Supplementary Fig. 7). When the energy source was changed from MW to conventional heating, the trend of increased decomposition rate and speed with increasing initial solution temperature remained consistent. At an initial solution temperature of 100 °C, where the effect of increasing solution temperature is negligible, the time required for complete degradation of 4-NP was 3 min for MW and 6 min for conventional heating, respectively. These results suggest that hotspot generation positively impacts the degradation process and that MW serves as a more efficient external energy source for catalyst activation compared to conventional heating.

The solution pH is a factor that affects the interaction between 4-NP and $CuFe_2O_4/Cu$. The pKa value of 4-NP is 7.15, indicating that the 4-NP form is predominant below this value, while the 4-nitrophenolate form becomes dominant above it 70 . The point of zero charge (PZC) for $CuFe_2O_4/Cu$ is at pH 9, which means the surface is positively charged below this value, neutral at pH 9, and negatively charged above it (Supplementary Fig. 8). Additionally, the zeta potential decreases with increasing pH, leading to a sharp increase in the hydrodynamic diameter of $CuFe_2O_4/Cu$ above pH 8. The interaction between 4-NP and $CuFe_2O_4/Cu$ was quantitatively confirmed through adsorption experiments of 4-NP at different pH values (Supplementary Fig. 9). At pH 4–7, the attractive forces between the positive charge on $CuFe_2O_4/Cu$ and the electron-donating groups of 4-NP result in

high adsorption. However, from pH 8 onwards, the decreasing surface area leads to a reduction in adsorption. At pH 10, adsorption is negligible due to electrostatic repulsion between CuFe $_2$ O $_4$ /Cu and 4-NP, as well as a further reduction in surface area. When the decomposition rate was examined at different pH values, rapid decomposition was observed at pH 4, but 4-NP could not be completely decomposed (Fig. 6f). The decomposition rate increased at pH levels between 5 and 7, with the most efficient performance observed at pH 7. Above pH 8, the decomposition rate decreased due to a reduction in surface area caused by catalyst aggregation. The MW-Fenton-like reaction cycle, which regenerates inactive forms into active forms, is a key factor in the generation of reactive oxygen species (ROS) and is influenced by both H⁺ and OH⁻ (Eqs. 3–6)⁷¹. Under neutral and near-neutral conditions (pH 7 and 8), the high degradation rates are likely due to the similar concentrations of H⁺ and OH⁻, which promote efficient operation of the cycle.

Recycle of CuFe₂O₄/Cu

Under optimal conditions (CuFe₂O₄/Cu 200 ppm, H_2O_2 200 ppm, 4-NP 10 ppm, 90 °C, pH 7, and 200 W) identified from previous experiments, the reusability of CuFe₂O₄/Cu was examined. It was observed that the decomposition rate remained consistent even after five cycles of the MW-Fenton-like reaction (Fig. 7a). Additionally, TEM images confirmed that the structure of the catalyst was maintained after five reactions (Supplementary Fig. 10). However, when conventional heating was used as an external energy source, the decomposition rate significantly decreased over the five cycles (Fig. 7b). TEM images revealed a reduction in catalyst density after repeated heat-Fenton-like reactions. This density reduction is believed to be due to metal leaching, which likely caused the decrease in the decomposition rate. ICP-OES measurements confirmed that the Cu leaching in the 1st cycle of the MW-Fenton-like reaction was 1.27 mg/L, which meets the US EPA



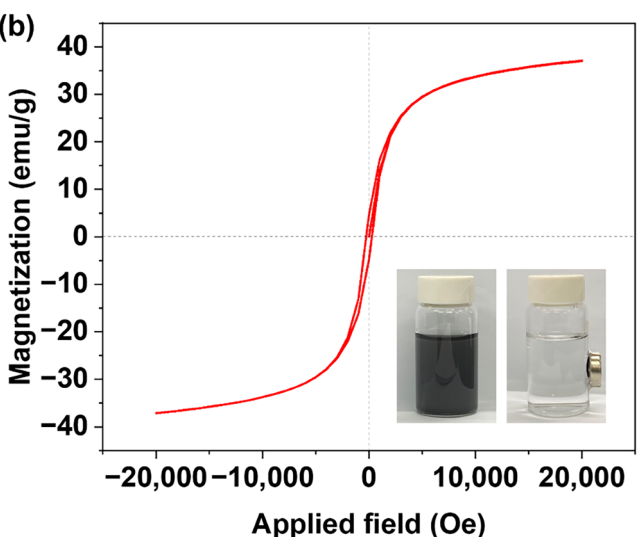


Fig. 4 | Degradation performance of commercial metal oxides and $CuFe_2O_4/Cu$ and magnetic property of $CuFe_2O_4/Cu$. a Degradation of 4-NP by MW-Fenton-like reaction with commercial metal oxides and synthesized $CuFe_2O_4/Cu$ (Initial experimental condition: Cat. 200 ppm, H_2O_2 200 ppm, 4-NP 10 ppm, 20 °C, pH 7, and 200 W) and **b** Hysteresis loop of $CuFe_2O_4/Cu$ at 295 K. The inserted picture shows the separation of $CuFe_2O_4/Cu$ dispersed in distilled water using a magnet.

effluent standard (1.3 mg/L) (Supplementary Table 3)⁷². In contrast, the Cu leaching in the 1st cycle of the heat-Fenton-like reaction was 4.13 mg/L, exceeding the standard. Both MW and heat conditions resulted in the highest Cu leaching in the 1st cycle, with decreasing amounts in subsequent cycles. Notably, in MW system, Cu leaching from the 2nd cycle onward was approximately 10% of the 1st cycle value and was considered negligible. For Fe, the leaching was 0 mg/L under all conditions, likely because the leached Fe formed precipitates that were filtered out during the solid separation process⁷³.

The catalyst's surface composition before and after the MW-Fenton-like reaction was analyzed using XPS. It was confirmed that there were no significant changes in the peaks of the XPS spectra despite the repeated reactions, as shown in Fig. 8a. In the Cu 2p spectra, peaks for Cu $^+$, Cu $^{2+}$, and the satellite were observed at 933.3, 934.9, and 943.0 eV, respectively. As the reaction progressed, Cu $^+$ increased from 25.0% to 59.7%, while Cu $^{2+}$ decreased from 48.8% to 23.1% (Fig. 8b). In addition, the Raman spectra showed the intensity changes of Cu $_2$ O and CuO, which corresponded to the XPS results (Supplementary Fig. 11) 74 . Despite the change in the Cu $^+$ /Cu $^{2+}$ ratio, the degradation efficiency was not significantly affected. These results

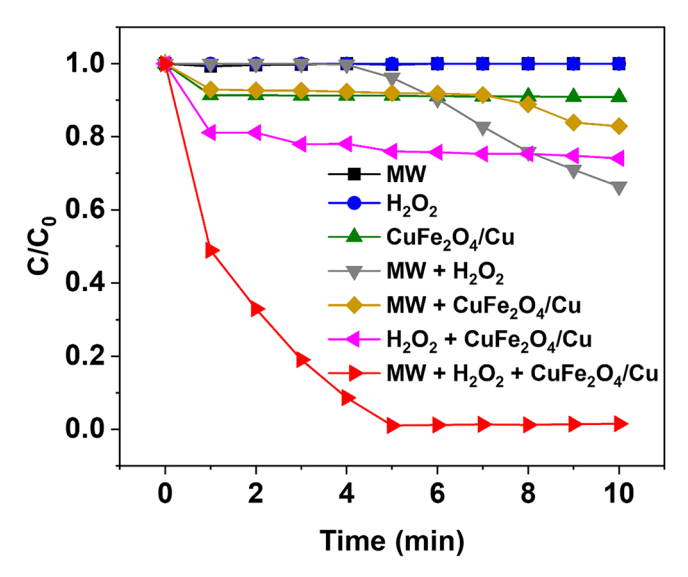


Fig. 5 | Degradation of 4-NP with respect to the combination of MW and Fenton-like reaction (Initial experimental condition: Cat. 200 ppm, $\rm H_2O_2$ 200 ppm, 4-NP 10 ppm, 20 °C, pH 7, and 200 W).

indicate that the reduction of Cu^{2+} to Cu^{+} (Eq. 4) is more prevalent than the oxidation of Cu⁺ to Cu²⁺ (Eq. 3) and confirm that Cu⁺ acts as the active species in the reaction. The Fe 2p spectra exhibited peaks at 710.8, 712.6, and 716.9 eV for Fe²⁺, Fe³⁺, and the satellite, respectively (Fig. 8c). During the reaction, Fe²⁺ increased from 32.2% to 35.2%, and Fe³⁺ decreased from 53.9% to 50.5%, with the peak shifting towards the lower binding energy. Based on the pattern of changes observed in the Cu spectra, this suggests that the reduction reaction of Fe ions (Eq. 6) is more dominant than the oxidation reaction (Eq. 5). In contrast to Cu, which exhibited a change of over 20%, Fe showed only about a 5% change, demonstrating that Cu has a more significant impact on 4-NP degradation than Fe. Peaks for lattice oxygen, surface oxygen, and absorbed water oxygen were identified in the O 1s spectra at 530.0, 531.3, and 532.2 eV, respectively (Fig. 8d). During the repetition of reactions, the oxygen in the lattice decreased from 50.7% to 43.8%, while the oxygen on the surface increased from 28.6% to 33.8%. In response to the peak shifts to lower binding energies observed in the Cu 2p and Fe 2p spectra, it appears that oxygen in the lattice is released to maintain the neutrality of the catalyst. The detailed XPS parameters for the MW-Fenton-like reaction samples can be found in Supplementary Table 4. Unlike the MW-Fenton-like reaction, samples subjected to the heat-Fentonlike reaction showed the disappearance of the Cu peak after five cycles in the Cu 2p spectra (Supplementary Fig. 12). The Raman spectra also showed a huge intensity decrease of Cu₂O and CuO compared to the MW-Fentonlike reaction sample (Supplementary Fig. 11). The results from XPS, Raman, and ICP-OES consistently reveal significant Cu leaching during the heat-Fenton-like reaction. The results indicate that the synthesized CuFe₂O₄/Cu catalyst demonstrates high stability and efficiency even after repeated reactions. Additionally, MW is demonstrated to be a more suitable external energy source than conventional heating for maintaining the catalyst's stability.

Degradation of 4-nitrophenol by MW-Fenton-like reaction

In the process of removing 4-NP through the MW-Fenton-like reaction, ROS generated by $\text{CuFe}_2\text{O}_4/\text{Cu}$ include 'OH, 'O $_2^-$, and h^+ . To investigate the impact of each ROS on 4-NP degradation, trapping experiments were conducted using DMSO, EDTA, and BQ (Fig. 9a). DMSO, EDTA, and BQ were used as scavengers for 'OH, h^+ , and 'O $_2^-$, respectively. Experimental results indicated that the contributions to 4-NP degradation were in the following order: 'OH $>h^+>\text{O}_2^-$. In particular, trapping 'OH resulted in a decrease of approximately 80% in the degradation rate, suggesting that 'OH is primarily responsible for most of the degradation.

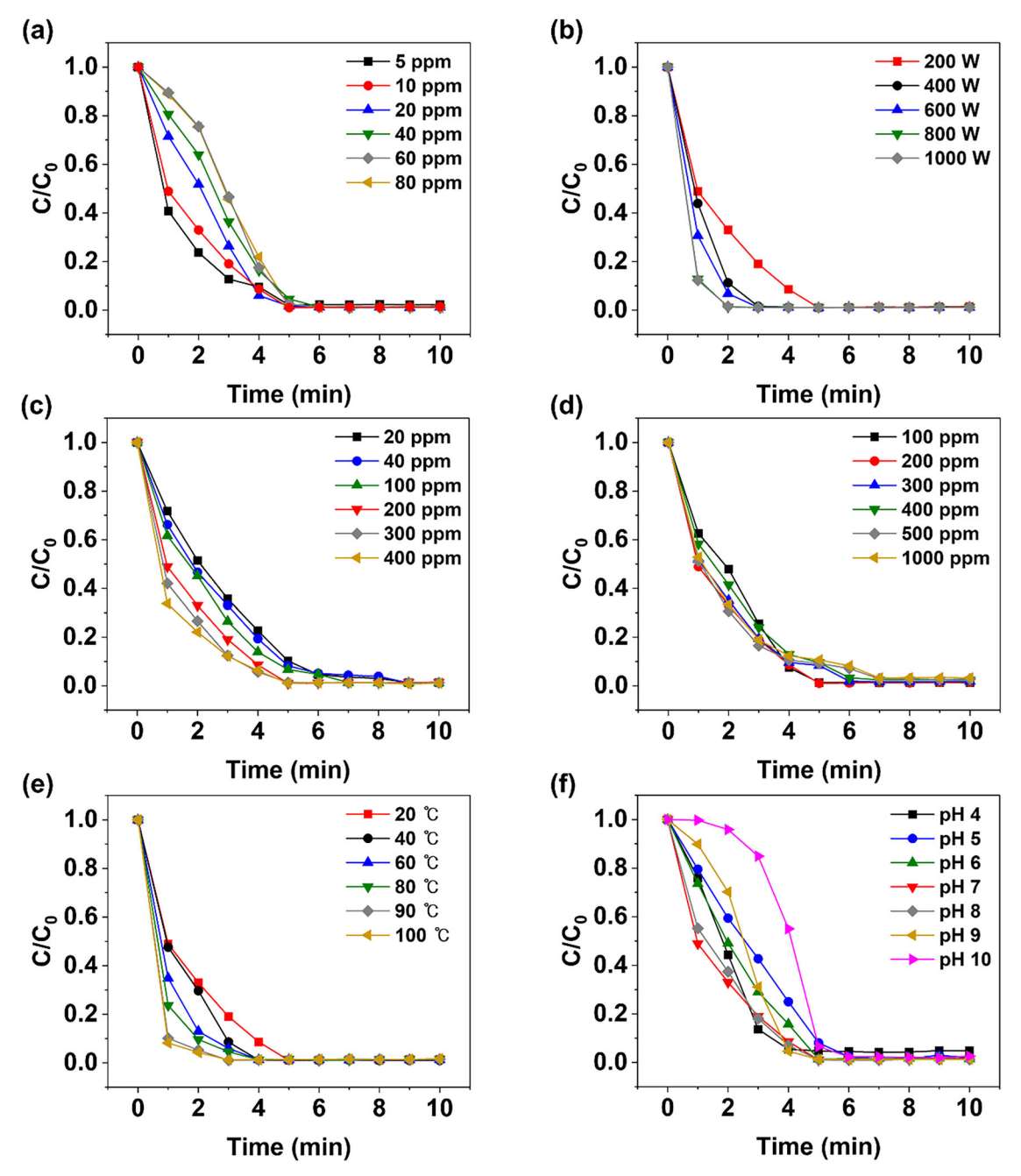


Fig. 6 | Degradation performance of 4-NP by MW-Fenton-like reaction according to experimental factor. a Effect of 4-NP concentration, b Effect of MW power, c Effect of $CuFe_2O_4/Cu$ concentration, d Effect of H_2O_2 concentration,

 $\bf e$ Effect of initial solution temperature, and $\bf f$ Effect of pH. Except for the control factor, others were maintained under the following conditions: Cat. 200 ppm, $\rm H_2O_2$ 200 ppm, 4-NP 10 ppm, 20 °C, pH 7, and 200 W.

The mechanism by which $CuFe_2O_4/Cu$ generates ROS through the MW-Fenton-like reaction is illustrated in Fig. 9b. $CuFe_2O_4/Cu$ generates $\cdot OH$ and $\cdot O_2^-$ through a Fenton-like reaction, where H_2O_2 acts as either an oxidizing or reducing agent (Eqs. 3–6). In the control experiment investigating the effects of pH, the pH values after the reaction showed a decreasing trend at all pH levels except pH 4 (Supplementary Table 5). And, higher degradation rates were observed under neutral and mildly basic conditions (pH 7 and 8) (Fig. 6f). This suggests that the reactions in Eqs. 4 and 6, which generate H^+ , play a more dominant role than those in Eqs. 3 and 5. Furthermore, the decrease in the ratio of high-valent Cu and Fe (Cu^{2+}/Fe^{3+}) and the increase in the ratio of low-valent Cu and Fe (Cu^{2+}/Fe^{3+}) after the MW-Fenton-like reaction also support this prediction (Fig. 8b, c). The $\cdot O_2H$ generated in Eqs. 4 and 6 is converted into H_2O_2 , O_2 , and OH^- through Eqs. 7 and 8, with $\cdot O_2^-$ acting as an intermediate 29,75 . MW has low energy, making

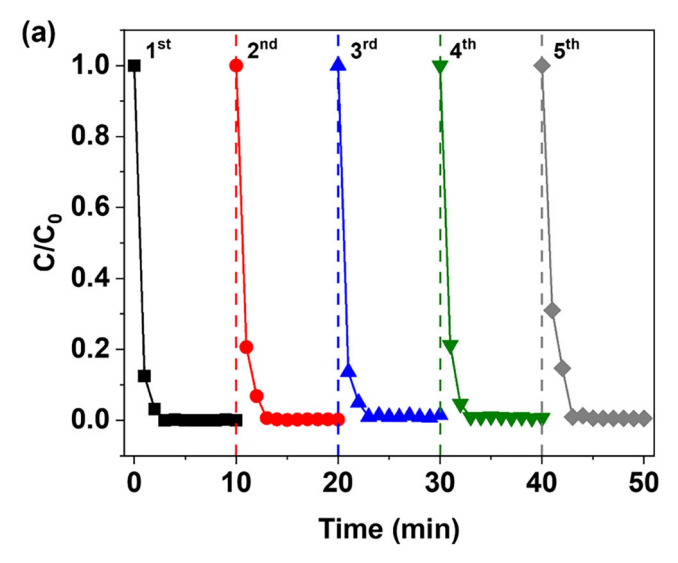
it insufficient to break chemical bonds or excite electrons from the valence band (VB) to the conduction band (CB)⁷⁶. However, with the increase in temperature and the formation of hotspots due to MW irradiation, the possibility of electron excitation also increases (Eq. 9)⁷⁷. The generated h^{*} and e⁻ react with OH⁻ and O₂ to produce ·OH and ·O₂⁻ (Eqs. 10 and 11)⁷⁸.

$$Cu^{+} + H_{2}O_{2} \rightarrow Cu^{2+} + \cdot OH + OH^{-}$$
 (3)

$$Cu^{2+} + H_2O_2 \rightarrow Cu^+ + \cdot O_2H + H^+$$
 (4)

$$Fe^{2+} + H_2O_2 \rightarrow Fe^{3+} + \cdot OH + OH^-$$
 (5)

$$Fe^{3+} + H_2O_2 \rightarrow Fe^{2+} + O_2H + H^+$$
 (6)



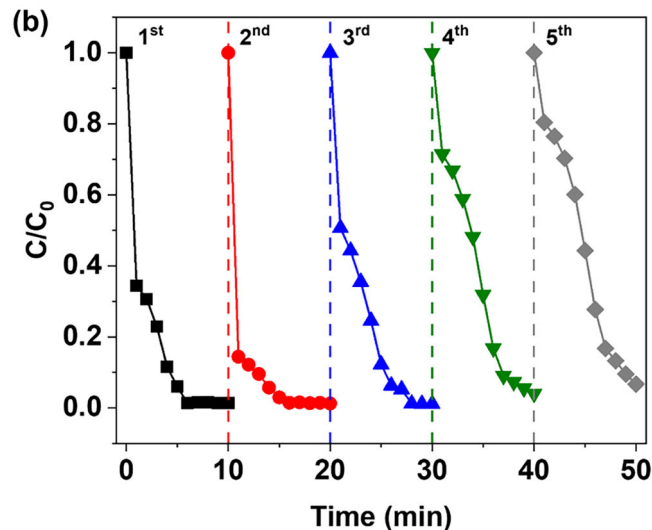


Fig. 7 | Recycling performance of CuFe₂O₄/Cu according to external energy type. a Consecutive degradation runs of MW-Fenton-like reaction (Initial experimental condition: Cat. 200 ppm, $\rm H_2O_2$ 200 ppm, 4-NP 10 ppm, 90 °C, pH 7, and 200 W) and b Consecutive degradation runs of heat-Fenton-like reaction (Initial experimental condition: Cat. 200 ppm, $\rm H_2O_2$ 200 ppm, 4-NP 10 ppm, 90 °C, and pH 7).

$$\cdot O_2 H \rightarrow \cdot O_2^- + H^+ \tag{7}$$

$$2 \cdot O_2^- + 2H_2O \rightarrow O_2 + H_2O_2 + 2OH^-$$
 (8)

Heated
$$CuFe_2O_4/Cu + MW \rightarrow h^+ in VB + e^- in CB$$
 (9)

$$OH^{-} + h^{+} in VB \rightarrow \cdot OH$$
 (10)

$$e^{-} \text{ in CB} + O_2 \rightarrow \cdot O_2^{-} \tag{11}$$

The ROS generated through the MW-Fenton-like reaction degraded the majority of 4-NP within 5 min and removed 43% of TOC within 10 min (Supplementary Fig. 13). The reduction in TOC indicates that 4-NP was degraded and ultimately mineralized to $CO_2(g)$. To investigate the degradation pathway of 4-NP, LC-qTOF-MS analysis was performed at different reaction times (Fig. 10). Significant peaks were observed at m/z = 87, 108, and 138. The peak at m/z = 138 corresponds to the pollutant 4-NP, with its intensity decreasing over time and disappearing after 5 min. The peak at m/z = 108 is likely due to benzoquinone (BQ) (m/z = 107) and hydroquinone

(HQ) (m/z = 109). When \cdot OH attacks the C-4 position of 4-NP, NO₂ is removed, producing HQ. HQ can be converted to BQ through a reversible redox reaction⁷⁹, and the peak at m/z = 108 may arise from hydrogen bonding between HQ and BQ⁸⁰. OH preferentially attack the electrophilic sites of HQ and BQ, leading to aromatic ring cleavage. This process generates pyruvic acid, a three-carbon compound, which is subsequently detected as a peak at m/z = 87 in the mass spectrum. Furthermore, pyruvic acid undergoes further degradation by \cdot OH, ultimately being mineralized into CO₂. After 10 min of reaction, although 57% of the TOC remained in the solution, no peaks were observed in the mass spectra. The small molecules formed from the degradation of 4-NP, which are expected to contain 2 to 6 carbon atoms, were not observed via LC-MS due to their rapid degradation and low concentration. However, the mineralization process, in which these small molecules are ultimately converted to CO₂(g), is expected to occur at a slower rate in comparison.

Discussion

In this study, magnetic $CuFe_2O_4$ was developed and synthesized into a spherical form of $CuFe_2O_4/Cu$, which was used as a catalyst in MW-Fenton-like reactions. Unlike Fe^{2+}/Fe^{3+} typically used in highly acidic environments, the synthesized $CuFe_2O_4/Cu$ functioned effectively across a wide pH range (4–10) and demonstrated the highest efficiency at neutral pH. Under the optimal conditions as determined from control experiments ($CuFe_2O_4/Cu$ 200 ppm, H_2O_2 200 ppm, 4-NP 10 ppm, 90 °C, pH 7, and 200 W), 4-NP was completely degraded. In repeated MW-Fenton-like reaction experiments with magnetic separation, $CuFe_2O_4/Cu$ maintained its degradation efficiency. This contrasts with the significant decline observed in heat-Fenton-like reaction experiments, demonstrating the superior catalyst stability under MW conditions. These results suggest that $CuFe_2O_4/Cu$ is a suitable catalyst for MW-Fenton-like reactions and holds promise for effective removal of various organic pollutants.

Methods Materials

The cobalt(II, III) oxide nanopowder (<50 nm, 99.5%), copper(II) oxide (<10 µm, 98%), iron(II, III) oxide (50–100 nm, 97%), copper iron oxide (<100 nm, 98.5%), zirconium(IV) oxide, iron(III) oxide (<5 μ m, \geq 96%), hafnium oxide (98%), niobium(V) oxide (99.9%), vanadium(V) oxide, 4-nitrophenol (ReagentPlus®, ≥99%), sodium hydroxide (ACS reagent, ≥97.0%), sodium bicarbonate (ACS reagent, ≥99.7%), hexadecyltrimethylammonium bromide (CTAB), ethylenediaminetetraacetic acid (EDTA, ACS reagent), p-benzoquinone (BQ, reagent grade), and dimethyl sulfoxide (DMSO, analytical standard) were purchased from Sigma-Aldrich. Bismuth(III) oxide (99.0%), magnesium oxide, glycerol, H₂O₂ (34.5%), copper(II) nitrate trihydrate, iron(III) nitrate nonahydrate, and HNO₃ (68.0-70.0%) were obtained from Samchun. From Kojundo Chemical Laboratory, yttrium(III) oxide (7 µm, 99.9%), cerium(IV) oxide (0.2 μm, 99.99%), chromium(III) oxide (3 μm, 99.9%), lanthanum(III) oxide (99.99%), gallium(III) oxide (99.99%), and manganese(III) oxide (99.9%) were purchased. Manganese(IV) oxide and nickel(II) oxide (99.0%) were gained from Junsei Chemical. Aluminum oxide (135 nm, 99.9%) was purchased from Any One Co., Ltd. TiO₂ (99.9%) and Sn₂O₃ (99.9%) were obtained from Grand Chemical & Material Co., Ltd. 2-Propanol was gained from JT Baker. The deionized (DI) water used in the experiment was ultrapure, with a resistance of 18.2 M Ω , sourced from Milli-Q water (C9209, Millipore Sigma, USA).

Synthesis of CuFe₂O₄ sphere

CuFe₂O₄ spheres are synthesized using a solvothermal method 81 . 1 mmol of CTAB, 0.25 mmol of Cu(NO₃)₂·3H₂O, and 0.5 mmol of Fe(NO₃)₃·9H₂O are dissolved in a solution containing 80 mL of isopropanol and 16 mL of glycerol. After stirring for 1 h, the solution was transferred to a 180 mL Teflon-lined stainless-steel autoclave and subjected to solvothermal treatment at 180 °C for 6 h. The synthesized CuFe glycerate was washed three times with ethanol and dried at 40 °C for 24 h. The dried CuFe glycerate was

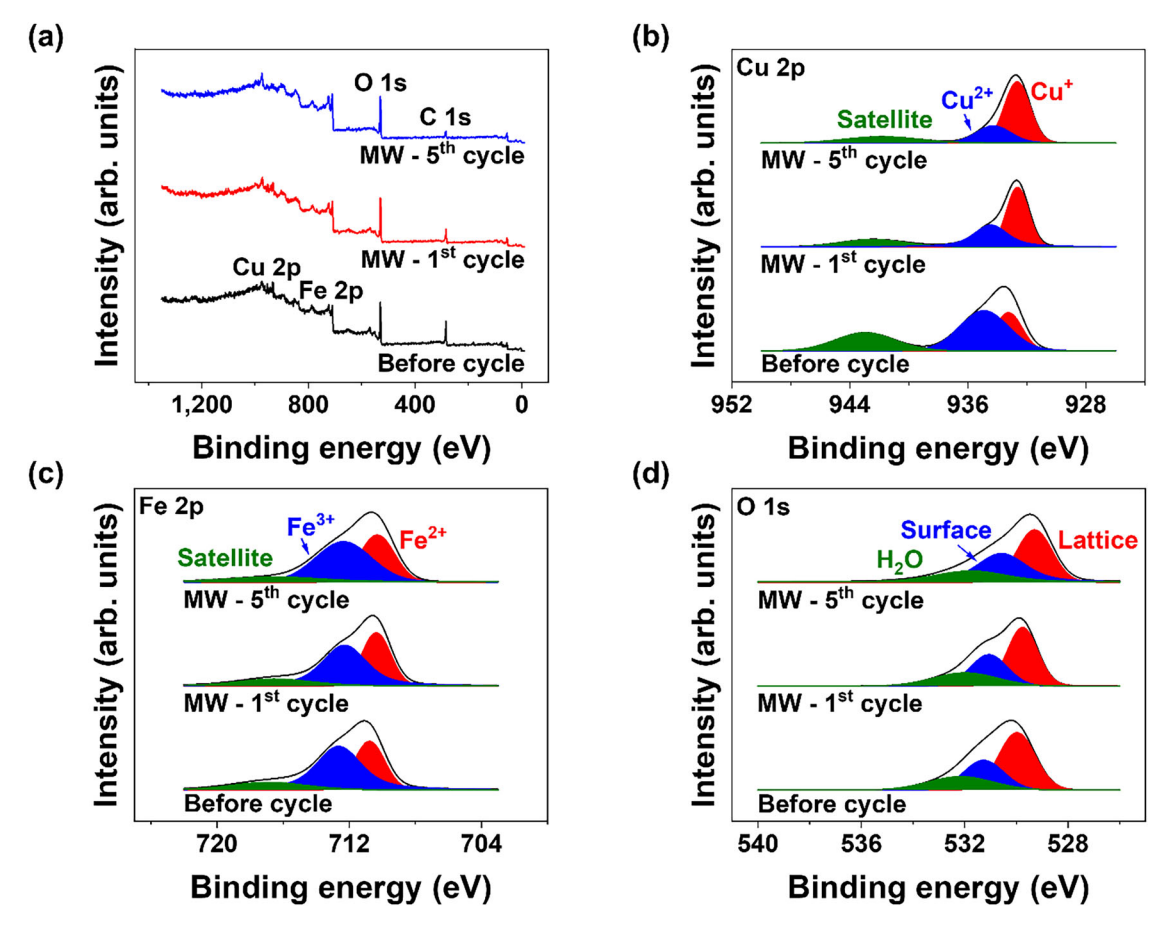


Fig. 8 | XPS spectra of CuFe₂O₄/Cu before, after 1 time, and 5 times of MW-Fenton-like reaction. a Survey spectra and fine-scanned spectra of b Cu 2p, c Fe 2p, and d O 1s.

heat-treated in an Ar atmosphere, with a ramp-up rate of 12 °C/min to 350 °C and held for 2 h to obtain $\text{CuFe}_2\text{O}_4/\text{Cu}$. By adjusting parameters such as the volume ratio of isopropanol to glycerol (110:14), the presence of CTAB, the solvothermal synthesis time (12 h), gas conditions (O $_2$ or Air), and the heating temperature (300 °C), different forms including spherical CuFe_2O_4 , $\text{CuFe}_2\text{O}_4/\text{Fe}_2\text{O}_3$, and $\text{CuFe}_2\text{O}_4/\text{CuO}$ were obtained.

Characterization

The morphology and size of the synthesized CuFe₂O₄ were analyzed using a Field Emission Scanning Electron Microscope (FESEM, SU5000, HITA-CHI, Japan) and a Transmission Electron Microscope (TEM, Tecnai G2 F30 S-Twin, FEI, USA). X-ray Diffraction (XRD, MiniFlex600, Rigaku, Japan) was used to confirm the crystallinity of CuFe₂O₄. The magnetic properties of the particles were verified through measurements with a Superconducting Quantum Interference Device (SQUID, MPMS XL, Quantum Design Inc., USA) at 295 K. X-ray Photoelectron Spectroscopy (XPS, Sigmaprobe, Thermo Fisher Scientific, UK) with a photon energy of 1486.6 eV (Al Kα) was employed for both quantitative and qualitative surface analysis before and after the experiment. Raman Spectroscopy (in Via Raman Microscope, Renishaw, UK) with a 633 nm laser was used to identify the chemical bonds features. A Dynamic Light Scattering instrument (DLS, Zetasizer Ultra Red Label, Malvern Panalytical Ltd., UK) with a 10 mW He-Ne laser measured the particle diameter and zeta potential in water. The amount of metal leached after the reaction was determined using Inductively Coupled Plasma Optical Emission Spectrometry (ICP-OES, ICPE-9000, Shimadzu, Japan). The concentration of 4-NP were monitored at 400 nm using UV-Vis Spectrophotometry (Cary 60 UV-Vis Spectrophotometer, Agilent, USA)⁷⁰. The residual carbon content in the solution after the reaction was determined using Total Organic Carbon analysis (TOC, TNM-L, Shimadzu, Japan). The intermediates formed during the decomposition of 4-NP were analyzed using a Liquid Chromatography Quadrupole Time-of-Flight Mass Spectrometer (LC-QTOF-MS, impact II, Bruker, USA) with a C18 column (100 mm \times 2.1 mm, Intensity Sole2, Bruker, USA). The system operated in negative electrospray ionization mode, with a 30:70 methanol:water mixture flowing at 0.2 mL/min.

Degradation of 4-nitrophenol

To investigate the effects of pH, CuFe₂O₄/Cu concentration, H₂O₂ concentration, pollutant concentration, initial solution temperature, and MW power, a series of experiments were designed. All variables were kept at baseline conditions (CuFe₂O₄/Cu 200 ppm, H₂O₂ 200 ppm, 4-NP 10 ppm, 20 °C, pH 7, and 200 W) except for the one being tested. A total solution volume of 50 mL was prepared in an Erlenmeyer flask, containing CuFe₂O₄/Cu (20-400 ppm), H₂O₂ (100-1000 ppm), and 4-NP (5-80 ppm) in DI water. The initial solution temperature (20-100 °C) was set using an electric kettle (FLE-03C, Fellow, USA). An ultrasonic bath (CPX2800H-E, EMERSON, USA) was used to disperse the CuFe₂O₄/Cu particles in the solution. The pH of the solution (pH 4–10) was adjusted using NaOH and HNO3 solutions prepared in three concentrations (0.01, 0.1, and 1 M), with pH maintained at an accuracy of \pm 0.1. The flask was placed in a microwave (MW23GD, LG Electronics Tianjin Applications Co., Ltd., Korea) connected to a condenser. To prevent loss of DI water due to temperature rise during the reaction, cooling water was circulated through the condenser using a pump (75211-15, Cole-Parmer Instrument Company, USA). The MW power (200–1000 W) was adjusted, and samples of 1.2 mL were taken at 1-min intervals for a total reaction time of 10 min. The collected samples were centrifuged at 13,500 rpm for 2 min using a centrifuge (MaXpin C-12mt, DAIHAN Scientific Co., Ltd., Korea) to separate the CuFe₂O₄/Cu particles. A clean supernatant of 0.6 mL was mixed with 0.6 mL of NaOH to prepare samples for UV-Vis analysis. The concentration of 4-NP was determined by measuring the absorbance at 400 nm⁷⁰.

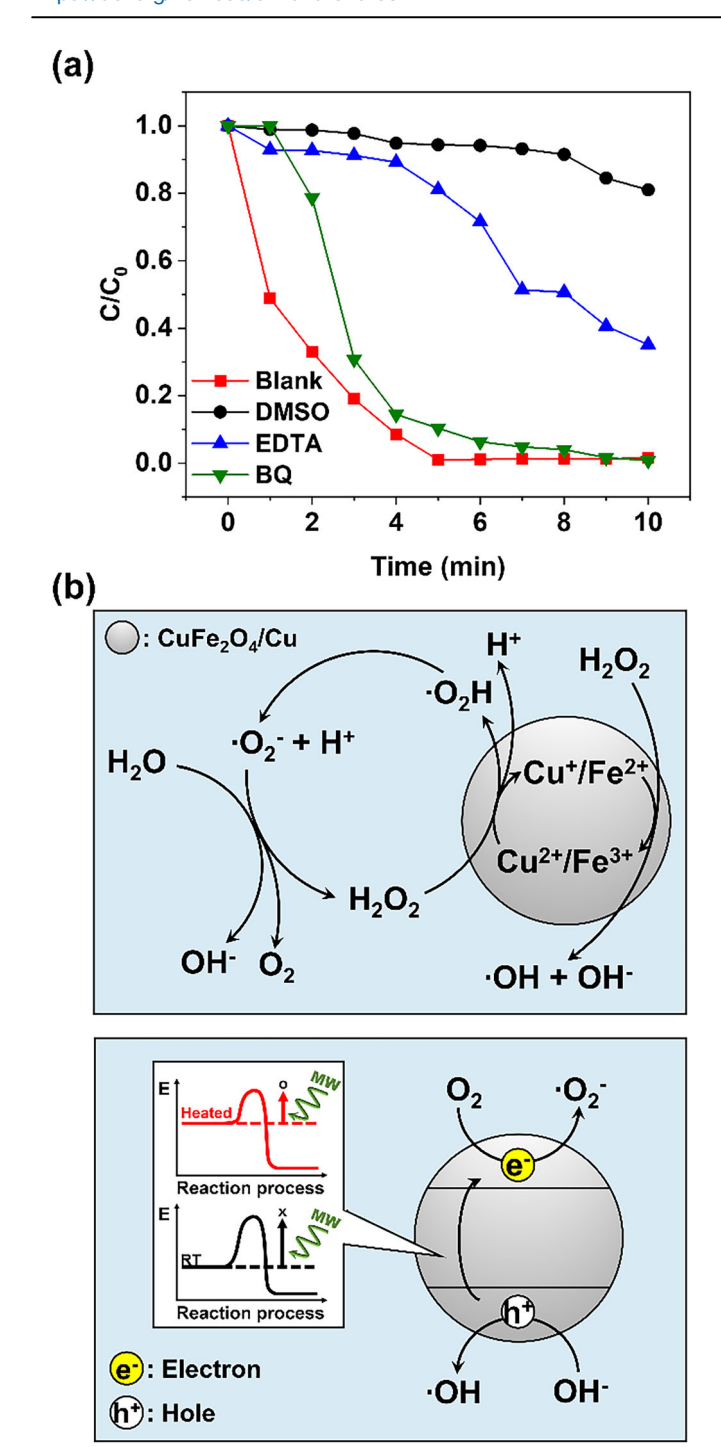


Fig. 9 | ROS identification and proposed mechanism in MW-Fenton-like reaction with CuFe₂O₄/Cu. a ROS trapping experiment of MW-Fenton-like reaction with CuFe₂O₄/Cu (Initial experimental condition: Cat. 200 ppm, H₂O₂ 200 ppm, 4-NP 10 ppm, 20 °C, pH 7, and 200 W). DMSO, EDTA, and BQ are used as ·OH, h^+ , and ·O₂ $^-$ trapping reagents. b Scheme of mechanism that can generate ·OH, h^+ , and ·O₂ $^-$ during MW-Fenton-like reaction with CuFe₂O₄/Cu.

Effect of external energy type

To compare the efficiency of MW and conventional heating as external energy sources, the MW reactor was replaced with a heating mantle (100A-0406, Glas-Col, USA). All other experimental conditions were kept constant, including CuFe₂O₄/Cu at 200 ppm, H_2O_2 at 200 ppm, 4-NP at 10 ppm, and pH 7. The initial solution temperature (20–100 °C) was set using an electric kettle. During the 10 min of reaction time, the heating mantle and a temperature controller

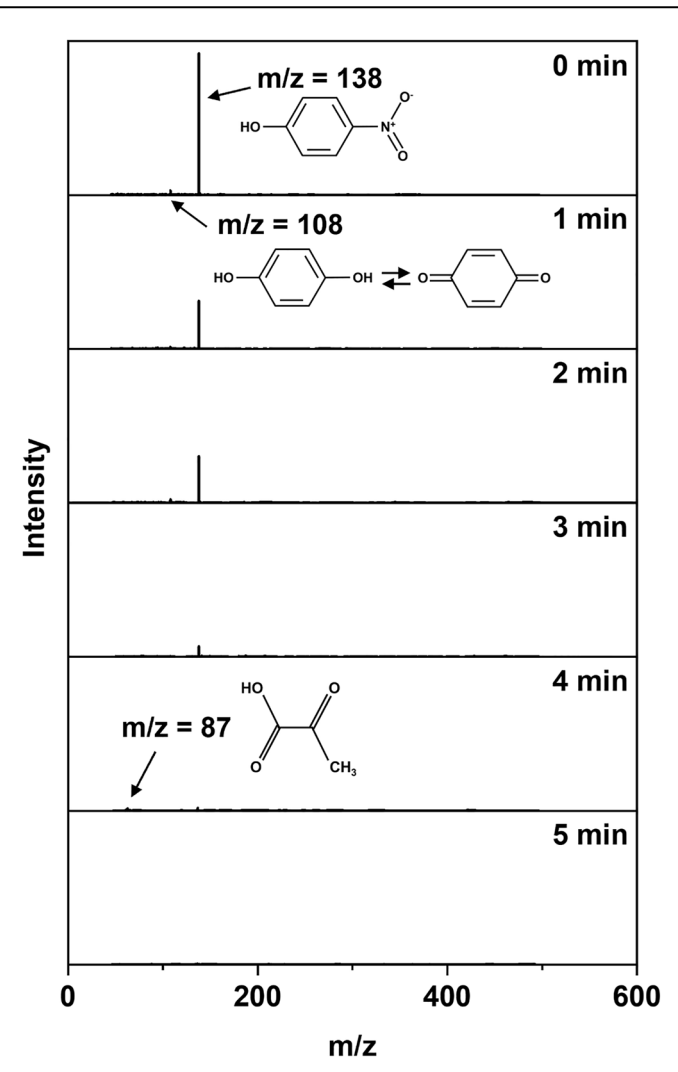


Fig. 10 | Mass spectrum of 4-NP with respect to the reaction time (Initial experimental condition: Cat. 200 ppm, $\rm H_2O_2$ 200 ppm, 4-NP 10 ppm, 20 °C, pH 7, and 200 W).

(TXN-700, AS ONE, Japan) maintained the solution temperature within \pm 3 °C. The experimental procedures and measurements followed the same protocols as the 4-NP degradation experiments using MW.

Recycle of CuFe₂O₄/Cu

Under the optimal conditions determined from the 4-NP degradation experiment (CuFe₂O₄/Cu 200 ppm, H₂O₂ 200 ppm, 4-NP 10 ppm, 90 °C, pH 7, and 200 W), a catalyst recycling experiment was conducted. The experimental procedure followed the same steps as the degradation experiment, with an additional washing process between each of the five reaction cycles to remove residual H₂O₂ and 4-NP. The washing process was designed to minimize catalyst loss using a magnet. The catalyst remaining in the microtubes was collected in an Erlenmeyer flask. The catalyst was allowed to settle by gravity and magnetic attraction, and then immobilized using a magnet. Subsequently, 35 mL of the supernatant was removed and replaced with an equal volume of DI water. This washing cycle was repeated 4 times. After the washing process, the sample was prepared with a solution matching the optimal conditions for the next cycle of the experiment.

Reporting summary

Further information on research design is available in the Nature Research Reporting Summary linked to this article.

Data availability

Data will be made available on request.

Received: 5 February 2025; Accepted: 9 May 2025; Published online: 01 July 2025

References

- Dai, W. et al. Study on the removal characteristics and degradation pathways of highly toxic and refractory organic pollutants in real pharmaceutical factory wastewater treated by a pilot-scale integrated process. Front. Microbiol. 14, 1128233. https://doi.org/10.3389/ fmicb.2023.1128233 (2023).
- Muszyński, A. et al. Cosmetic wastewater treatment with combined light/Fe⁰/H₂O₂ process coupled with activated sludge. *J. Hazard. Mater.* 378, 120732. https://doi.org/10.1016/j.jhazmat.2019.06.009 (2019).
- Azanaw, A., Birlie, B., Teshome, B. & Jemberie, M. Textile effluent treatment methods and eco-friendly resolution of textile wastewater. Case Stud. Chem. Environ. Eng. 6, 100230. https://doi.org/10.1016/j. cscee.2022.100230 (2022).
- Wiedeman, A. in Produced water 2: environmental issues and mitigation technologies 27-41 (Springer, 1996)
- Preisner, M., Neverova-Dziopak, E. & Kowalewski, Z. An analytical review of different approaches to wastewater discharge standards with particular emphasis on nutrients. *Environ. Manag.* 66, 694–708, https://doi.org/10.1007/s00267-020-01344-y (2020).
- Gómez, T., Gémar, G., Molinos-Senante, M., Sala-Garrido, R. & Caballero, R. Assessing the efficiency of wastewater treatment plants: A double-bootstrap approach. J. Clean. Prod. 164, 315–324, https://doi.org/10.1016/j.jclepro.2017.06.198 (2017).
- Zhang, M.-H., Dong, H., Zhao, L., Wang, D.-X. & Meng, D. A review on Fenton process for organic wastewater treatment based on optimization perspective. Sci. Total Environ. 670, 110–121, https:// doi.org/10.1016/j.scitotenv.2019.03.180 (2019).
- Jorge, N., Teixeira, A. R., Gomes, A., Lucas, M. S. & Peres, J. A. Sulfate radical advanced oxidation processes: activation methods and application to industrial wastewater treatment. *Eng. Proc.* 56, 162, https://doi.org/10.3390/ASEC2023-15500 (2023).
- Jain, B., Singh, A. K., Kim, H., Lichtfouse, E. & Sharma, V. K. Treatment of organic pollutants by homogeneous and heterogeneous Fenton reaction processes. *Environ. Chem. Lett.* 16, 947–967, https://doi. org/10.1007/s10311-018-0738-3 (2018).
- Wang, S. A comparative study of Fenton and Fenton-like reaction kinetics in decolourisation of wastewater. *Dyes Pigments* 76, 714–720, https://doi.org/10.1016/j.dyepig.2007.01.012 (2008).
- Abdullah, N., Karsiti, M. & Ibrahim, R. A review of pH neutralization process control. 2012 4th International Conference on Intelligent and Advanced Systems (ICIAS2012). 594-598; https://doi.org/10.1109/ ICIAS.2012.6306084 (2012).
- Dutta, K., Mukhopadhyay, S., Bhattacharjee, S. & Chaudhuri, B. Chemical oxidation of methylene blue using a Fenton-like reaction. *J. Hazard. Mater.* 84, 57–71, https://doi.org/10.1016/S0304-3894(01) 00202-3 (2001).
- Tang, J. & Wang, J. Iron-copper bimetallic metal-organic frameworks for efficient Fenton-like degradation of sulfamethoxazole under mild conditions. Chemosphere 241, 125002. https://doi.org/10.1016/j. chemosphere.2019.125002 (2020).
- Kim, Y., Dumett Torres, D. & Jain, P. K. Activation energies of plasmonic catalysts. *Nano Lett.* 16, 3399–3407, https://doi.org/10. 1021/acs.nanolett.6b01373 (2016).
- 15. Bokhari, A., Yusup, S., Asif, S., Chuah, L. F. & Michelle, L. Z. Y. in *Bioreactors* 27-42 (Elsevier, 2020).
- Bagaria, P. et al. A comprehensive decomposition analysis of stabilization energy (CDASE) and its application in locating the rate-

- determining step of multi-step reactions. *Phys. Chem. Chem. Phys.* **11.** 8306–8315, https://doi.org/10.1039/B902335F (2009).
- Zhu, Y. et al. Strategies for enhancing the heterogeneous Fenton catalytic reactivity: A review. Appl. Catal. B: Environ. 255, 117739. https://doi.org/10.1016/j.apcatb.2019.05.041 (2019).
- Goats, G. Microwave diathermy. Br. J. Sports Med. 24, 212, https://doi.org/10.1136/bjsm.24.4.212 (1990).
- Xia, H. et al. A review of microwave-assisted advanced oxidation processes for wastewater treatment. *Chemosphere* 287, 131981. https://doi.org/10.1016/j.chemosphere.2021.131981 (2022).
- Bermúdez, J., Beneroso, D., Rey-Raap, N., Arenillas, A. & Menéndez, J. Energy consumption estimation in the scaling-up of microwave heating processes. *Chem. Eng. Process.* 95, 1–8, https://doi.org/10. 1016/j.cep.2015.05.001 (2015).
- Yang, Y., Wang, P., Shi, S. & Liu, Y. Microwave enhanced Fenton-like process for the treatment of high concentration pharmaceutical wastewater. *J. Hazard. Mater.* 168, 238–245, https://doi.org/10.1016/ j.jhazmat.2009.02.038 (2009).
- Li, S., Zhang, G., Wang, P., Zheng, H. & Zheng, Y. Microwave-enhanced Mn-Fenton process for the removal of BPA in water. *Chem. Eng. J.* 294, 371–379, https://doi.org/10.1016/j.cej.2016.03.006 (2016).
- Wang, N., Zheng, T., Jiang, J. & Wang, P. Cu(II)–Fe(II)–H₂O₂ oxidative removal of 3-nitroaniline in water under microwave irradiation. *Chem. Eng. J.* 260, 386–392, https://doi.org/10.1016/j.cej.2014.09.002 (2015).
- Iboukhoulef, H., Amrane, A. & Kadi, H. Optimization of phenolic compounds abatement in olive mill wastewater by Fenton's-like treatment with H₂O₂/Cu²⁺ under microwave using experimental design. *Environ. Eng. Manage. J.* 17, https://doi.org/10.30638/eemj. 2018.125 (2018).
- Xu, D., Cheng, F., Lu, Q. & Dai, P. Microwave enhanced catalytic degradation of methyl orange in aqueous solution over CuO/CeO₂ catalyst in the absence and presence of H₂O₂. *Ind. Eng. Chem. Res.* 53, 2625–2632, https://doi.org/10.1021/ie4033022 (2014).
- Pan, W., Zhang, G., Zheng, T. & Wang, P. Degradation of p-nitrophenol using CuO/Al₂O₃ as a Fenton-like catalyst under microwave irradiation. *RSC Adv.* 5, 27043–27051, https://doi.org/10. 1039/C4RA14516J (2015).
- Cai, M.-Q. et al. Rapid decolorization of dye Orange G by microwave enhanced Fenton-like reaction with delafossite-type CuFeO₂. Sci. Total Environ. 580, 966–973, https://doi.org/10.1016/j.scitotenv. 2016.12.047 (2017).
- Zhang, B., You, H. & Wang, F. Microwave-enhanced catalytic wet peroxide oxidation of quinoline: the influence of pH and H₂O₂ dosage and identification of reactive oxygen species. *RSC Adv.* 7, 14769–14775, https://doi.org/10.1039/C7RA01350G (2017).
- Qi, Y. et al. Highly efficient microwave-assisted Fenton degradation of metacycline using pine-needle-like CuCo₂O₄ nanocatalyst. *Chem. Eng. J.* 373, 1158–1167, https://doi.org/10.1016/j.cej.2019.05.097 (2019).
- Tony, M. & Mansour, S. A. Microwave-assisted catalytic oxidation of methomyl pesticide by Cu/Cu₂O/CuO hybrid nanoparticles as a Fenton-like source. *Int. J. Environ. Sci. Technol.* 17, 161–174, https://doi.org/10.1007/s13762-019-02436-x (2020).
- Ghorbanian, Z., Asgari, G., Samadi, M. T. & Seid-mohammadi, A. Removal of 2, 4 dichlorophenol using microwave assisted nanoscale zero-valent copper activated persulfate from aqueous solutions: Mineralization, kinetics, and degradation pathways. J. Mol. Liq. 296, 111873. https://doi.org/10.1016/j.molliq.2019.111873 (2019).
- Gouasmia, A., Zouaoui, E., Mekkaoui, A. A., Haddad, A. & Bousba, D. Highly efficient photocatalytic degradation of malachite green dye over copper oxide and copper cobaltite photocatalysts under solar or microwave irradiation. *Inorg. Chem. Commun.* 145, 110066. https:// doi.org/10.1016/j.inoche.2022.110066 (2022).

- Bose, S. & Kumar, M. Microwave responsive copper-ferrite (CuFe₂O₄)
 encapsulated in molybdenum-disulfide (MoS₂) nanoflower catalyst
 for antibiotic removal via persulfate oxidation. Surf. Interfaces 49,
 104428. https://doi.org/10.1016/j.surfin.2024.104428 (2024).
- Nam, Y. et al. Hollow sphere CuCo₂O₄ as highly efficient catalyst of microwave-assisted Fenton-like reaction for water treatment. *J. Water Process Eng.* 60, 105116. https://doi.org/10.1016/j.jwpe.2024. 105116 (2024).
- Vieira, Y. et al. CuFeS₂/activated carbon heterostructure as a microwave-responsive catalyst for reductive and oxidative degradation of ibuprofen, ketoprofen, and diclofenac. *Chem. Eng. J.* 480, 148060. https://doi.org/10.1016/j.cej.2023.148060 (2024).
- Wang, Y., Wang, R., Lin, N., Wang, Y. & Zhang, X. Highly efficient microwave-assisted Fenton degradation bisphenol A using iron oxide modified double perovskite intercalated montmorillonite composite nanomaterial as catalyst. J. Colloid Interface Sci. 594, 446–459, https://doi.org/10.1016/j.jcis.2021.03.046 (2021).
- Yingzhe, Z. et al. The synthesis of Cu/Fe/Fe₃O₄ catalyst through the aqueous solution ball milling method assisted by high-frequency electromagnetic field. Superlatt. Microstruct. 118, 123–129, https:// doi.org/10.1016/j.spmi.2018.04.016 (2018).
- Pandey, N. et al. Exploration of copper-cysteamine nanoparticles as an efficient heterogeneous Fenton-like catalyst for wastewater treatment. *Mater. Today Phys.* 22, 100587. https://doi.org/10.1016/j. mtphys.2021.100587 (2022).
- Shen, T. et al. Application of nickel foam supported Cu–MnO₂ in microwave enhanced Fenton-like process for p-nitrophenol removal: Degradation, synergy and mechanism insight. *J. Clean. Prod.* 397, 136442. https://doi.org/10.1016/j.jclepro.2023.136442 (2023).
- Xiao, J., Fang, X., Yang, S., He, H. & Sun, C. Microwave-assisted heterogeneous catalytic oxidation of high-concentration Reactive yellow 3 with CuFe₂O₄/PAC. *J. Chem. Technol. Biotechnol.* 90, 1861–1868, https://doi.org/10.1002/jctb.4497 (2015).
- Yao, X. et al. Degradation of humic acid using hydrogen peroxide activated by CuO-Co₃O₄@AC under microwave irradiation. *Chem. Eng. J.* 330, 783–791, https://doi.org/10.1016/j.cej.2017.08.008 (2017)
- Liu, Z. et al. Highly efficient degradation of phenol wastewater by microwave induced H₂O₂-CuO_x/GAC catalytic oxidation process. Sep. Purif. Technol. 193, 49–57, https://doi.org/10.1016/j.seppur. 2017.11.010 (2018).
- 43. Li, Z. et al. Preparation and properties of Cu-Ni bimetallic oxide catalyst supported on activated carbon for microwave assisted catalytic wet hydrogen peroxide oxidation for biologically pretreated coal chemical industry wastewater treatment. *Chemosphere* 214, 17–24, https://doi.org/10.1016/j.chemosphere.2018.09.098 (2019).
- Yao, T. et al. One-step preparation of reduced graphene oxide aerogel loaded with mesoporous copper ferrite nanocubes: A highly efficient catalyst in microwave-assisted Fenton reaction. *J. Hazard. Mater.* 378, 120712. https://doi.org/10.1016/j.jhazmat.2019.05.105 (2019).
- Vieira, Y., Ceretta, M. B., Foletto, E. L., Wolski, E. A. & Silvestri, S. Application of a novel rGO-CuFeS₂ composite catalyst conjugated to microwave irradiation for ultra-fast real textile wastewater treatment. J. Water Process Eng. 36, 101397. https://doi.org/10.1016/j.jwpe. 2020.101397 (2020).
- Xia, G., Sun, J., Yang, W., Wu, G.-L. & Shen, W. Studies on the reaction mechanism of Cu/SiC catalytic oxidation for degradation of methyl orange in presence of microwave. *Water Sci. Technol.* 79, 1164–1173, https://doi.org/10.2166/wst.2019.114 (2019).
- Liu, X. et al. Ofloxacin degradation over Cu–Ce tyre carbon catalysts by the microwave assisted persulfate process. *Appl. Catal. B: Environ.* 253, 149–159, https://doi.org/10.1016/j.apcatb.2019.04.047 (2019).
- Sun, J., Xia, G., Yang, W., Hu, Y. & Shen, W. Microwave-assisted method to degrade phenol using persulfate or hydrogen peroxide

- catalyzed by Cu-bearing silicon carbide. Water Sci. Technol. 82, 704–714. https://doi.org/10.2166/wst.2020.370 (2020).
- 49. Wang, Y., Yu, L., Wang, R., Wang, Y. & Zhang, X. Reactivity of carbon spheres templated Ce/LaCo_{0.5}Cu_{0.5}O₃ in the microwave induced H₂O₂ catalytic degradation of salicylic acid: Characterization, kinetic and mechanism studies. *J. Colloid Interface Sci.* 574, 74–86, https://doi.org/10.1016/j.jcis.2020.04.042 (2020).
- Wang, Y. et al. Efficient reactivity of LaCu_{0.5}Co_{0.5}O₃ perovskite intercalated montmorillonite and g-C₃N₄ nanocomposites in microwave-induced H₂O₂ catalytic degradation of bisphenol A. *Chem. Eng. J.* 401, 126057. https://doi.org/10.1016/j.cej.2020. 126057 (2020).
- Wang, Y., Yu, L., Wang, R., Wang, Y. & Zhang, X. Microwave catalytic activities of supported perovskite catalysts MO_x/
 LaCo_{0.5}Cu_{0.5}O₃@CM (M=Mg, Al) for salicylic acid degradation. *J. Colloid Interface Sci.* 564, 392–405, https://doi.org/10.1016/j.jcis. 2019.12.130 (2020).
- Gogoi, D., Karmur, R. S., Das, M. R. & Ghosh, N. N. Cu and CoFe₂O₄ nanoparticles decorated hierarchical porous carbon: An excellent catalyst for reduction of nitroaromatics and microwave-assisted antibiotic degradation. *Appl. Catal. B: Environ.* 312, 121407. https://doi.org/10.1016/j.apcatb.2022.121407 (2022).
- Zhang, Q. et al. Efficient microwave-assisted mineralization of oxytetracycline driven by persulfate and hypochlorite over Cu-biochar catalyst. *Bioresour. Technol.* 372, 128698. https://doi.org/10.1016/j. biortech.2023.128698 (2023).
- Wang, Y. et al. Construction of microwave/PMS combined dual responsive perovskite-MXene system for antibiotic degradation: synergistic effects of thermal and non-thermal. *Appl. Surf. Sci.* 639, 158263. https://doi.org/10.1016/j.apsusc.2023.158263 (2023).
- Pang, H. et al. Research advances in composition, structure and mechanisms of microwave absorbing materials. *Compos. Part B: Eng.* 224, 109173. https://doi.org/10.1016/j.compositesb.2021. 109173 (2021).
- Leshuk, T. et al. Magnetic flocculation for nanoparticle separation and catalyst recycling. *Environ. Sci. Nano* 5, 509–519, https://doi.org/10. 1039/C7EN00827A (2018).
- Makarchuk, O., Dontsova, T., Perekos, A., Skoblik, A. & Svystunov, Y. Magnetic mineral nanocomposite sorbents for wastewater treatment. *J. Nanomater.* 2017, 8579598. https://doi.org/10.1155/2017/8579598 (2017).
- Shukla, S., Khan, R. & Daverey, A. Synthesis and characterization of magnetic nanoparticles, and their applications in wastewater treatment: A review. *Environ. Technol. Innov.* 24, 101924. https://doi. org/10.1016/j.eti.2021.101924 (2021).
- Mmelesi, O. K. et al. Effect of Zn doping on physico-chemical properties of cobalt ferrite for the photodegradation of amoxicillin and deactivation of E. coli. *Colloids Surf. A Physicochem. Eng. Asp.* 649, 129462. https://doi.org/10.1016/j.colsurfa.2022.129462 (2022).
- Mmelesi, O. et al. Synthesis of cobalt ferrite in one-pot-polyol method, characterization, and application to methylparaben photodegradation in the presence of peroxydisulfate. *Mater. Today Chem.* 26, 101029. https://doi.org/10.1016/j.mtchem.2022.101029 (2022).
- Li, Z., Guo, C., Lyu, J., Hu, Z. & Ge, M. Tetracycline degradation by persulfate activated with magnetic Cu/CuFe₂O₄ composite: efficiency, stability, mechanism and degradation pathway. *J. Hazard. Mater.* 373, 85–96, https://doi.org/10.1016/j.jhazmat.2019.03.075 (2019).
- Zhao, B. et al. Degradation of 4-nitrophenol (4-NP) using Fe–TiO₂ as a heterogeneous photo-Fenton catalyst. *J. Hazard. Mater.* 176, 569–574, https://doi.org/10.1016/j.jhazmat.2009.11.066 (2010).
- 63. Zeng, X., Cheng, X., Yu, R. & Stucky, G. D. Electromagnetic microwave absorption theory and recent achievements in microwave

- absorbers. Carbon 168, 606–623, https://doi.org/10.1016/j.carbon. 2020.07.028 (2020).
- Wang, B., Wu, Q., Fu, Y. & Liu, T. A review on carbon/magnetic metal composites for microwave absorption. *J. Mater. Sci. Technol.* 86, 91–109, https://doi.org/10.1016/j.jmst.2020.12.078 (2021).
- Hou, T. et al. A review of metal oxide-related microwave absorbing materials from the dimension and morphology perspective. *J. Mater. Sci.: Mater. Electron.* 30, 10961–10984, https://doi.org/10.1007/s10854-019-01537-0 (2019).
- Zhang, X. J., Guo, A. P., Wang, G. S. & Yin, P. G. Recent progress in microwave absorption of nanomaterials: composition modulation, structural design, and their practical applications. *IET Nanodielectr.* 2, 2–10, https://doi.org/10.1049/iet-nde.2018.0014 (2019).
- Bokare, A. D. & Choi, W. Review of iron-free Fenton-like systems for activating H₂O₂ in advanced oxidation processes. *J. Hazard. Mater.* 275, 121–135, https://doi.org/10.1016/j.jhazmat.2014.04.054 (2014).
- Liu, J., Xie, H. & Hu, X. Fenton-like catalytic oxidation of o-cresol wastewater by H₂O₂ over Fe₂O₃/AC catalysts. *Mater. Res. Express* 8, 095506, https://doi.org/10.1088/2053-1591/ac2283 (2021).
- Mohammed, N. A., Alwared, A. I. & Salman, M. S. Photocatalytic degradation of reactive yellow dye in wastewater using H₂O₂/TiO₂/UV technique. *Iraqi J. Chem. Petrol. Eng.* 21, 15–21, https://doi.org/10. 31699/JJCPE.2020.1.3 (2020).
- Tiar, K., Soualah, A., Bisio, C. & Guidotti, M. Effect of initial solution pH on 4-nitrophenol oxidation through homogeneous/heterogeneous photo-Fenton process using goethite/H₂O₂ system. *J. Photochem. Photobiol. A: Chem.* 447, 115184. https://doi.org/10.1016/j.jphotochem.2023.115184 (2024).
- Guo, X., Wang, K. & Xu, Y. Tartaric acid enhanced CuFe₂O₄-catalyzed heterogeneous photo-Fenton-like degradation of methylene blue. *Mater. Sci. Eng. B* 245, 75–84, https://doi.org/10.1016/j.mseb.2019. 05.015 (2019).
- Quiton, K. G. N., Huang, Y.-H. & Lu, M.-C. Recovery of cobalt and copper from single-and co-contaminated simulated electroplating wastewater via carbonate and hydroxide precipitation. *Sustain. Environ.* Res. 32, 31, https://doi.org/10.1186/s42834-022-00140-z (2022).
- Pham, A. N., Rose, A. L., Feitz, A. J. & Waite, T. D. Kinetics of Fe(III) precipitation in aqueous solutions at pH 6.0–9.5 and 25 °C. Geochim. Cosmochim. Acta 70, 640–650, https://doi.org/10.1016/j.gca.2005. 10.018 (2006).
- Wu, F., Myung, Y. & Banerjee, P. Rayleigh instability driven nodular Cu₂O nanowires via carbothermal reduction of CuO nanowires. *Cryst. Growth Des.* 15, 1588–1595, https://doi.org/10.1021/cg500784y (2015).
- Liu, L., Li, Y., Pang, Y., Lan, Y. & Zhou, L. Activation of peroxymonosulfate with CuCo₂O₄@kaolin for the efficient degradation of phenacetin. *Chem. Eng. J.* 401, 126014. https://doi. org/10.1016/j.cej.2020.126014 (2020).
- Qiu, Y. et al. Highly efficient microwave catalytic oxidation degradation of p-nitrophenol over microwave catalyst of pristine α-Bi₂O₃. Chem. Eng. J. 306, 667–675, https://doi.org/10.1016/j.cej. 2016.06.133 (2016).
- Liu, X., An, S., Shi, W., Yang, Q. & Zhang, L. Microwave-induced catalytic oxidation of malachite green under magnetic Cu-ferrites: new insight into the degradation mechanism and pathway. *J. Mol. Catal. A: Chem.* 395, 243–250, https://doi.org/10.1016/j.molcata. 2014.08.028 (2014).
- Qiu, Y. & Zhou, J. Highly effective and green microwave catalytic oxidation degradation of nitrophenols over Bi₂O₂CO₃ based composites without extra chemical additives. *Chemosphere* 214, 319–329, https://doi.org/10.1016/j.chemosphere.2018.09.125 (2019).

- Ye, R., Henkensmeier, D. & Chen, R. Imidazolium cation enabled reversibility of a hydroquinone derivative for designing aqueous redox electrolytes. Sustain. Energy Fuels 4, 2998–3005, https://doi.org/10. 1039/D0SE00409J (2020).
- Gamboa-Valero, N. et al. Hydrogen bonding complexes in the quinone-hydroquinone system and the transition to a reversible twoelectron transfer mechanism. *Electrochim. Acta* 188, 602–610, https://doi.org/10.1016/j.electacta.2015.12.060 (2016).
- Jiang, S.-F., Wang, L. L., Hu, W.-F., Tian, K. & Jiang, H. Preparation of flower-like CuFe₂O₄ by a self-templating method for high-efficient activation of peroxymonosulfate to degrade carbamazepine. *Ind. Eng. Chem. Res.* 60, 11045–11055, https://doi.org/10.1021/acs.iecr. 1c02254 (2021).

Acknowledgements

This work was supported by the National Research Foundation of Korea (NRF) grant funded by the Korea government (MSIT) (No. RS-2022-NR071792), and the Gwangju Institute of Science and Technology (GIST) research fund (Future-leading Specialized Research Project, 2025).

Author contributions

Y.N.: Conceptualization, Data curation, Formal analysis, Investigation, Methodology, Visualization, Writing – original draft. D.N.: Data curation, Formal analysis, Investigation, Writing – review and editing. Y.M.: Data curation, Formal analysis, Supervision, Writing – review and editing. J.J.: Resources, Writing – review and editing. C.K.: Funding acquisition, Project administration, Supervision, Writing – review and editing. All authors contributed to this study as described above.

Competing interests

The authors declare no competing interests.

Additional information

Supplementary information The online version contains supplementary material available at https://doi.org/10.1038/s41545-025-00477-z.

Correspondence and requests for materials should be addressed to Changwoo Kim.

Reprints and permissions information is available at http://www.nature.com/reprints

Publisher's note Springer Nature remains neutral with regard to jurisdictional claims in published maps and institutional affiliations.

Open Access This article is licensed under a Creative Commons Attribution 4.0 International License, which permits use, sharing, adaptation, distribution and reproduction in any medium or format, as long as you give appropriate credit to the original author(s) and the source, provide a link to the Creative Commons licence, and indicate if changes were made. The images or other third party material in this article are included in the article's Creative Commons licence, unless indicated otherwise in a credit line to the material. If material is not included in the article's Creative Commons licence and your intended use is not permitted by statutory regulation or exceeds the permitted use, you will need to obtain permission directly from the copyright holder. To view a copy of this licence, visit http://creativecommons.org/licenses/by/4.0/.

© The Author(s) 2025